Clays and Clay Minerals, Vol. 59, No. 1, 58–74, 2011.

CHARACTER AND AMOUNT OF I-S MIXED-LAYER MINERALS AND PHYSICAL-CHEMICAL PARAMETERS OF TWO CERAMIC CLAYS FROM WESTERWALD, GERMANY: IMPLICATIONS FOR PROCESSING PROPERTIES

Kerstin Petrick[1,2], Ralf Diedel[3], Miriam Peuker[3], Matthias Dieterle[4], Paul Kuch[4], René Kaden[2], Peter Krolla-Sidenstein[2], Rainer Schuhmann[1,2], and Katja Emmerich[1,2]

[1] Competence Center for Material Moisture (CMM), KIT-Karlsruhe Institute of Technology, 76021 Karlsruhe, Germany
[2] Institute for Functional Interfaces (IFG), KIT-Karlsruhe Institute of Technology, 76021 Karlsruhe, Germany
[3] FGK Forschungsinstitut für Anorganische Werkstoffe-Glas/Keramik-GmbH, 56203 Höhr-Grenzhausen, Germany
[4] WBB Fuchs, 56412 Ruppach-Goldhausen, Germany

Abstract—The industrial assessment of ceramic clays commonly consists of the determination of just two parameters, the particle-size distribution and the chemical composition; other parameters may also be important, however. The aim of the present study was to show that a careful determination of the mineralogical phase content provides valuable additional information on the processing behavior of ceramic clays.

Two ceramic clays (W1 and W2) from the Westerwald area, Germany, were evaluated as being the same with respect to industrial screening criteria, but showed different processing properties. In order to elucidate the different behaviors, both clays were investigated comprehensively using a multi-method approach combining physical-chemical and mineralogical methods.

Different aggregation characteristics for the two clays were revealed by determining the grain-size distribution with and without Na-pyrophosphate as a dispersant. In addition, W1 showed a greater electrical conductivity and soluble-salt concentration which promoted dispersion behavior.

The phase content was identified both for bulk materials and for several grain-size fractions by X-ray diffraction (XRD) and Rietveld analysis. The quantitative phase content was crosschecked with the chemical composition by X-ray fluorescence (XRF) analysis. Additional information was gathered by thermal analysis, cation exchange capacity (CEC) measurements, Mössbauer spectroscopy, and optical microscopy. While bulk samples of W1 and W2 showed nearly the same mineralogical and chemical compositions, investigation of the clay-size fractions (0.6−2 μm, <0.6 μm) revealed differences in the composition of the 2:1 layer silicates. The percentages of smectite in the mixed-layer I-S, as well as the amount of kaolinite, discrete illite, and smectite were determined by one-dimensional XRD profile fitting (ODPF). Best-fitting results for W1 were achieved for a physical mixture of an illite-rich I-S mixed-layer mineral (R3 I(0.9)-S) with discrete smectite, whereas W2 was characterized by a greater proportion of smectite in the mixed-layer (R1 I(0.8)-S), without discrete smectite. Based on the different structural features of the swellable clays, a qualitative delamination model for the 2:1 layer silicates during processing of the clays was derived. The model provides a further approach, aside from aggregation characteristics, to help understand the clay-processing behavior, which was found to be different for the two ceramic clays investigated.

Key Words—Ceramic Clays, Delamination, Germany, Illite-smectite, Interstratification, Mixed-layer Minerals, Multi-method Approach, Processing Properties, Westerwald, XRD Profile Fitting.

INTRODUCTION

Ceramic clays are used in a wide variety of applications, from high-quality tableware and sanitary ware to electrical porcelain, glazes, and tiles. These uses are governed by several factors including the geological and geochemical conditions under which the clays were formed and transformed (mineralogical composition), and the physical and chemical properties (Murray, 2000). The mineralogical composition is widely believed to control the ceramic-processing related properties (Schmidt, 1981). However, relations established between properties and components in mineralogical systems take into account the main components only (Schüller, 1980). As summarized by Kaufhold and Penner (2006), the amount and nature of swelling clay minerals (smectite and smectitic components in illite-smectite mixed-layer minerals) exert a strong influence on the workability of the clays, including properties such as viscosity (Störr, 1983), 'making moisture' content (Hofmann, 1962), plasticity (Kromer and Rose, 1994), dry-bending strength (Wiegmann *et al*., 1978; Schüller, 1980), and shrinkage (Kromer and Schüller, 1973; Wiegmann *et al*., 1978; Störr and Schwerdtner, 1979). Despite the well known influence of mineral composition, the quality of raw clays for industrial application is still evaluated merely by the chemical composition

* E-mail address of corresponding author:
kerstin.petrick@kit.edu
DOI: 10.1346/CCMN.2011.0590108

(Schejbal, 1978) and grain-size distribution (Winkler, 1954).

The mineralogical composition of ceramic clays is characterized by varying amounts of finely dispersed quartz, feldspars (mostly K-feldspars, albite/oligoclase), micas (often referred to as sericite*, muscovite, and illite), kaolinite, Fe(oxyhydr)oxides, and occasionally varying portions of mixed-layer minerals such as illite-smectite. In addition, several clays contain very finely distributed organic matter and lignite, which is sometimes mineralized (marcasite) (Kromer, 1979, 1980). Westerwald ceramic clays have a complex composition due to the coexistence of different clay minerals, mainly illite, illite-smectite mixed-layer minerals (I-S), smectite, and kaolinite with varying degrees of disorder (Kaufhold and Penner, 2006). The characterization of such complex clay mixtures remains a challenge (Omotoso *et al*., 2006; Kleeberg, 2009). Quantitative XRD analysis of the smectite content using the Rietveld method has been possible since 2006 using commercial software such as *AutoQuan* (by Seifert Analytical X-ray, version 2.7.0), based on smectite structure models developed by Ufer *et al*. (2004). To date, no appropriate structural model for illite-smectite mixed-layer minerals within the Rietveld method has been available, but is under development (Ufer *et al*., 2009).

The combination of different analytical methods (XRF, simultaneous thermal analysis – STA, CEC) in addition to Rietveld analysis of XRD patterns allows an approximation of the mineralogical phase content. One-dimensional XRD profile fitting (ODPF), previously used mainly in oil exploration-related identification of mixed-layer minerals and clay-mineral paragenesis (*e.g.* Środoń, 1981; Drits *et al*., 1997; Lindgreen *et al*., 2000; McCarty *et al*., 2008; Lanson *et al*., 2009), is now used as an analytical tool for ceramic clays. The ODPF technique enables the characterization of complex samples consisting of discrete clay minerals and mixed-layer phases. However, the application of one-dimensional modeling does not always provide an unambiguous determination of the actual structure as several structural models may fit the experimental data equally well (Drits, 1987; Sakharov *et al*., 1999; McCarty *et al*., 2004). Fitting results have to be evaluated critically by comparing them with the chemical and mineralogical analyses in order to obtain a consistent characterization.

Despite the known variations in properties due to the variability of mineralogical composition, even ceramic clays having similar compositions show different processing properties. Those differences can only be elucidated by a comprehensive mineralogical characterization by the advanced methods described above. In this context, two ceramic clays (W1 and W2), from the Westerwald area of Germany, with different processing properties, but apparently similar chemical and mineralogical composition, were investigated thoroughly. The different processing properties in terms of extruding behavior and 'making moisture' content could not be explained on the basis of the bulk material composition. As minor constituents exert a strong effect on processing properties (Schüller, 1980), a detailed characterization of the smectite layer content was required.

The aim of the study was to conduct a consistent mineralogical characterization by means of a multi-method approach which enables detection of processing-related differences between two ceramic clays which have been evaluated as being identical according to industrial clay assessment methods.

MATERIALS

Two sedimentary clays (W1 and W2) from the Westerwald area were investigated. The samples were taken from adjacent deposits: W1 from the 'Geigenflur' clay deposit and W2 from the 'Petschmorgen' clay deposit, both of which were formed by decomposition and weathering during the Tertiary (Eocene/Oligocene) on Devonian slates (Rhenish Massif). During the Miocene, the area was changed by volcanic activity. The warm volcanic waters ascending along the zones of weakness caused the alteration of volcanites and probably led to the formation of smectites (Kromer, 1980).

According to industrial assessment standards, clays W1 and W2 are identical in terms of their chemistry and particle-size distribution, but show different working properties in terms of extruding behavior (generally referred to as "plasticity" according to Göhlert and Uebel, 2007) and 'making moisture' content, which is the amount of water required to create a plastic clay. A phenomenological description of the two samples and their processing properties is given in Table 1.

Sampling

Five tons of each of the freshly mined clays W1 and W2 were mixed with tap water and homogenized in a processing plant. In order to obtain a plastic mass, the gravimetric water content was increased from ~12% in the natural state to ~15% with respect to the final bulk mass. The clays were then homogenized again. The large samples were taken to ensure representative sampling from each quarry and to carry out a clay-maturation experiment, discussed elsewhere (Menger-Krug *et al*., 2008; Petrick *et al*., 2008). For the experiment, part of each batch was divided into 15 buckets of 20 kg each. For the mineralogical characterization, each sample was reduced to 500 g by subsampling by means of coning

* sericite: according to Rieder *et al*. (1998) the use of this name for fine-grained aggregates of mica-like phases is discouraged.

Table 1. Phenomenological description and processing properties-related parameters of the Westerwald clays W1 and W2.

	W1	W2
Color	Gray	Cream
Average aggregate size of the starting material in pit-moist state	1–1.5 cm	~0.5 cm
Dispersibility in water	Easy to disperse	More difficult to disperse under the formation of a 'sticky' sediment
Processing behavior	Plastic	Less plastic
– extrusion	37 bar	23 bar
– 'making moisture' content	28.0%	26.5%

and quartering, and then using a rotating sample divider (Crosby and Patel, 1995).

Sample preparation

Two different pathways for sample preparation were followed. In the first, chemical dispersants were used as is standard in the procedures in ceramics for evaluating raw clay qualities and grain-size distribution (DIN 19683-2). The second pathway was designed for methods employing microbial processing by not using chemical dispersants, which could be harmful to the metabolic activity of the microorganisms (Krolla-Sidenstein *et al*., 2009; Liu *et al*., 1982).

Pathway 1 consisted of the dispersion of samples using Na-pyrophosphate as a dispersant prior to the determination of grain-size distribution. Twenty grams of the oven-dried (110ºC) samples were suspended in 100 mL of 0.002 M Na-pyrophosphate by stirring (500 rpm) and ultrasound irradiation (ELMA T460/H, 70 W, 35 kHz).

For pathway 2, 50 g of each sample with inherent moisture was suspended in 2 L of deionized water. Polyethylene (PE) bottles containing the suspensions were irradiated for 30 min in an ultrasonic bath (Sonorex Bandelin RK 514 BH, 215 W, 35 kHz) and then placed on an end-over-end shaker for 24 h. Afterwards W1 and W2 were grain-size fractionated. The >63 μm fraction was separated by wet-sieving. The 20–63 μm, 2–20 μm, and <2 μm fractions were obtained by sedimentation. Settling times were calculated according to Stokes' law. The <0.6 μm fraction was extracted from the <2 μm fraction by centrifugation at $1240 \times g$ (solid content <0.3%) for 10 min with h = 6 cm at 20ºC, which also yielded the 0.6–2 μm fraction For XRD measurements, part of the <0.6 μm fraction was Ca-saturated by adding a 4 M $CaCl_2$ solution (excess of 20 times the CEC) to the suspensions of 2.5% solid content. The suspensions were shaken for 24 h. After centrifugation, the supernatant was removed and the clay sediment was saturated again by dispersion in the $CaCl_2$ solution. The saturation step was repeated three times. The suspensions were then washed with deionized water until chloride free (conductivity of the supernatant <4 μS/cm). The Ca-saturated suspensions were oven dried at 60ºC.

METHODS

Physical-chemical methods

The 'making moisture' content was measured according to Pfefferkorn with a deformation ratio of 2.0 (Vogt and Vogt, 2004). No generally acknowledged method or measuring unit for this property is available, so the extruding behavior was determined as a function of radial pressure in a trapezoidal die (Göhlert and Uebel, 2007).

The working properties are closely related to pH and soluble-salt concentration (Penner and Lagaly, 2001). Hence, the pH of both bulk materials was determined on the basis of DIN 38 414-4 for six replicates. Five grams of each bulk material, previously dried at 40ºC for 24 h, was mixed with a 0.01 M $CaCl_2$ solution. The suspensions were shaken in PE bottles for 24 h. Centrifugation was carried out at $4350 \times g$, at T = 20ºC for 25 min. Afterward, the pH of the supernatant was determined under stirring using a KCl electrode (WTW SenTix 81, Wissenschaftlich-Technische Werkstätten, Weilheim, Germany). Electrical conductivity was measured simultaneously (WTW TetraCon 325, Wissenschaftlich-Technische Werkstätten, Weilheim, Germany). The values were read after 10 min.

The concentration of soluble salts by means of anions (Cl^-, SO_4^{2-}) was analyzed from six replicates by ion chromatography using a Dionex DX-120 device (Sunnyvale, California, USA).

Mineralogical water content (w_{min})

The gravimetric mineralogical water content, w_{min}, was determined, in duplicate, by weight loss at 105ºC for 24 h with respect to bulk mass.

Grain-size distribution

Grain-size distribution was determined by sedimentation analysis in two different ways. Mass-fraction measurements were carried out for pathway 1 according to industrial standards by means of an X-ray attenuation method using a Micromeritics MasterTech 52 Sedigraph III. In order to test the influence of the measuring method, an additional sedimentation analysis was carried out by pipette analysis (Loomis, 1938) for pathway 1,

employing Na-pyrophosphate as a dispersant. Following pathway 2 of sample preparation, each separated fraction was weighed.

X-ray diffraction

The XRD diffraction patterns were recorded using a Bruker D5000 diffractometer, equipped with a graphite secondary monochromator and scintillation detector, using CuKα radiation. Top-loaded powdered samples were measured at 0.02º2θ step intervals from 2 to 80º2θ with 3 s per step. The divergence and antiscatter slits were 1 mm and the detector slit was 0.1 mm.

The quantitative mineral content was determined by the Rietveld method (Bergmann *et al*., 1998) applying *AutoQuan* software.

Oriented sample preparation according to the multi-specimen method (Drits and Sakharov, 1976; Drits *et al*., 1997a; Sakharov *et al*., 1999) was applied for one-dimensional XRD pattern fitting. X-ray diffraction patterns of the same sample were recorded after each of the different treatments. Oriented samples were produced for the Ca-saturated samples by pipetting a suspension onto a glass slide and drying overnight under atmospheric conditions at room temperature. Air-dried samples (AD) were prepared at a thickness of 15 mg/cm^2 to prevent loss of intensity (Moore and Reynolds, 1997). Ethylene glycol (EG) solvation was achieved by exposing the slides to EG vapor at 60ºC for 24 h (Whitney and Northrop, 1987). Heat-treated samples were obtained by heating the slides at 375ºC for 3 h (Moore and Reynolds, 1997). The oriented samples were measured at 0.02º2θ step intervals from 2 to 30º2θ with 6 s per step. The divergence, antiscatter, and detector slits were the same as above.

Characterization of the clay minerals and the mixed-layer phases was performed by one-dimensional XRD profile fitting of the EG-solvated samples of the coarse clay fraction (0.6–2 μm) and the middle to fine clay fraction (<0.6 μm) using *SYBILLA* software (Zeelmaekers *et al*., 2007), which is based on the program by Drits and Sakharov (1976). σ* (the standard deviation of a Gaussian orientation function for the crystals in the powder aggregate) was set to 12 and the number of unit cells in a crystallite (T_{mean}) was kept between 3 and 14, as recommended by Moore and Reynolds (1997). The quality of agreement between the experimental and the calculated XRD patterns was evaluated by a profile factor R_p (Howard and Preston, 1989).

The degree of structural disorder of kaolinite was established by application of the Hinckley index (Hinckley, 1963).

X-ray fluorescence analysis

The chemical composition of the bulk material and the grain-size fractionated samples was determined by XRF analysis, using a MagiXPRO spectrometer from Philips. Fused pellets were prepared from 0.8–0.9 g of powdered ignited samples mixed with lithium tetraborate in a ratio of 1 to 7.

Simultaneous thermal analysis

Supplementary information on mineral identification and characterization was obtained by use of STA, a combination of Thermogravimetry (TG) and Differential Scanning Calorimetry (DSC), using a Netzsch 449C Jupiter STA coupled with a quadrupole mass spectrometer (QMS 430C Aeolos). Sample amounts of 100 mg were measured at a constant heating rate. Measuring conditions were taken from Wolters *et al*. (2009) and are summarized in Table 2. In order to ensure reproducibility in weighing, samples were stored at 53% relative humidity over a saturated solution of $Mg(NO_3)_2 \cdot 6H_2O$ (Koster van Groos and Guggenheim, 1984).

On the basis of the mass loss during the dehydroxylation reaction between 400 and 900ºC, the maximum possible clay content was estimated by comparing the measured mass loss from TG curves with the calculated mass loss based on the quantification results from Rietveld analysis.

Further information on the kaolinite structure was gathered by PA (from the German term *Probenabhängigkeit* meaning 'sample dependency') curves (Smykatz-Kloss, 1974). The PA curves display the dependency of the peak temperature of a decomposition reaction (*e.g*. dehydroxylation) from the applied mass during thermal analysis and differ for minerals with different degrees of structural disorder. The dehydroxylation temperature of kaolinite depends strongly on the degree of structural disorder. The PA curves were recorded and compared with well characterized samples of known degrees of structural disorder.

Measurement of the CEC and exchangeable cations

The CEC measurements were carried out photometrically both for the bulk material and for the clay fractions (0.6–2 μm, <0.6 μm) with 0.01 M Cu-triethylenetetramine (Meier and Kahr, 1999) in

Table 2. Experimental parameters for STA measurements.

	TG/DSC/MS
Quantity of sample	100 mg
Grain size	Powder <200 μm
Packing density	Loosely packed, no pressing
Reference material	Empty crucible with lid
Furnace atmosphere	50 mL/min air + 20 mL/min N_2
Crucibles	Pt/Rh with lid
Thermocouples	$Pt/Pt_{90}Rh_{10}$
Heating rate	10 K/min
Temperature range	35–1100ºC

Table 3. Grain-size distribution of samples W1 and W2 with and without Na-pyrophosphate as a dispersant, obtained from different methods.

Grain size fraction (μm)	With dispersant, Sedigraph (pathway 1) W1 (%)	With dispersant, Sedigraph (pathway 1) W2 (%)	With dispersant, pipette procedure (pathway 1) W1 (%)	With dispersant, pipette procedure (pathway 1) W2 (%)	Without dispersant, pipette procedure (pathway 2) W1 (%)	Without dispersant, pipette procedure (pathway 2) W2 (%)
>63	1	3	2	5	2	5
20–63	10	12	18	17	19	21
2–20	29	31	27	28	31	31
0.6–2	10	13	10	21	24	39
<0.6	50	41	43	29	24	4

order to estimate the maximum smectite layer content. The amount of exchanged ions (Na^+, Mg^{2+}, K^+, Ca^{2+}, Al^{3+}, Fe^{3+}) in the supernatant was determined by inductively coupled plasma optical emission spectrometry (ICP-OES) with a device from Horiba Jobin Yvon (JY 38 S).

Mössbauer spectroscopy

Insight into Fe valence and coordination state was gained through use of Mössbauer spectroscopy. Spectra were taken at 295 K and 4.2 K using a ^{57}Co in rhodium source. An absorber thickness of 200 mg/cm^2 was chosen because of the small Fe content of the samples. For experimental details see Wagner and Kyek (2004).

Microscopy

Particle morphology was examined by means of optical microscopy (Zeiss Discovery V12) and by means of environmental scanning electron microscopy (ESEM) using a Philips ESEM XL 30 FEG. The device was operated at an acceleration voltage of 15 kV and a chamber pressure of 1 Torr. For energy dispersive X-ray (EDX) measurements, a liquid nitrogen-cooled Sapphire Si(Li) detecting unit from EDAX was used. The collection time for each spectrum was between 2 and 10 min.

RESULTS

Grain-size distribution and processing properties-related parameters

The two samples studied had very similar water contents: W1 = 13.4% (s = 0.4%), W2 = 13.7% (s = 1.0%) where s is the standard deviation water-sample content as received from the processing plant. Considerable differences in grain-size distribution were noticed between the two pathways (Table 3). The use of Na-pyrophosphate led to a mass shift toward finer grain-size fractions, very significant for the <0.6 μm fraction for both samples. Regardless of pathway, W1 was characterized by a greater content in the <2 μm clay size fractions.

W1, referred to as plastic, had a larger 'making moisture' content and extrusion pressure value than the less-plastic sample W2 (Table 1).

The pH values of W1 and W2 were very similar within standard deviation: 6.1 (s = 0.8) for W1 and 6.9 (s = 0.7) for W2. The soluble-salt concentrations in terms of SO_4^{2-} and Cl^- anions were 479 mg/kg (s = 171 mg/kg) and 116 mg/kg (s = 13 mg/kg), respectively, for W1, and 37 mg/kg (s = 8 mg/kg) and 79 mg/kg (s = 5 mg/kg), respectively, for sample W2. The overall soluble-salt concentration of W1 was greater and this was reflected by a much greater electrical conductivity,

Table 4. Chemical compositions of the bulk materials for W1 and W2 and their respective clay fractions (0.6–2 μm and <0.6 μm). The values were normalized for loss on ignition (LOI).

	Chemical composition (%)					
	W1 bulk	W2 bulk	W1 0.6–2 μm	W2 0.6–2 μm	W1 <0.6 μm	W2 <0.6 μm
SiO_2	74.79	75.27	57.24	53.86	52.93	52.66
Al_2O_3	19.40	18.94	33.12	36.55	38.50	39.33
Fe_2O_3 (total)	1.54	1.44	1.99	2.24	2.71	1.95
MgO	0.43	0.45	0.72	0.81	0.79	0.89
CaO	0.28	0.22	0.37	0.36	0.61	0.63
Na_2O	0.12	0.09	0.28	0.21	0.25	0.24
K_2O	2.11	2.34	4.14	4.33	3.30	3.99
TiO_2	1.32	1.25	2.15	1.65	0.93	0.31
LOI	6.25	5.63	9.42	10.30	12.70	12.24

400 µS/cm (s = 99 µS/cm) compared to 51 µS/cm (s = 11 µS/cm) for W2.

X-ray techniques

Investigation of the bulk samples revealed that W1 and W2 had very similar chemical compositions (Table 4) and phase contents. The quantitative phase content of each of the bulk materials and of their 0.6−2 µm and <0.6 µm clay fractions (summarized in Table 5) revealed that they were composed mainly of quartz, kaolinite, illite, swellable components (*i.e.* I-S mixed-layer minerals and/or discrete smectite), orthoclase, plagioclase, and rutile, as well as small quantities of Fe-bearing phases.

As expected, the amount of layer silicates increased with decreasing grain size, whereas the amount of quartz decreased. The amount of feldspar and rutile remained constant within the various grain-size fractions.

In order to check the quantification results from Rietveld analysis, the mineralogical phase content was converted to chemical composition in terms of element oxides and then these values were compared with the chemical compositions from XRF measurements. A positive relative deviation between the two data sets (Figure 1) means an underestimation by Rietveld quantification; a negative deviation denotes overestimation. In the clay fractions of both samples, a considerable increase in terms of deviation was noted. For W1, the increase was magnified in the <0.6 µm fraction, whereas W2 exhibited the strongest deviations in the 0.6−2 µm size fraction. The Al_2O_3 content showed both overestimation for the bulk materials and underestimation for the clay fractions.

The XRD patterns of the clay fractions (0.6−2 µm and <0.6 µm) from the oriented-sample preparation look very similar at first glance (Figure 2) with strong reflections at 7.14 Å and 3.57 Å from kaolinite and a non-rational series of basal reflections with d_{001} at ~10 Å. These values differed slightly from a rational series for illite and are diagnostic of mixed-layer I-S species. After EG solvation, changes in the diffraction patterns of all samples were noted: peak shift in the region between 7 and 8º2θ and broadening of the peak at 17.7º2θ indicated the presence of a smectite component. The identification of mixed-layer I-S species was confirmed by the heat-treated samples, the XRD patterns of which resembled a physical mixture of a pure illite and kaolinite.

The morphology of the I-S basal reflections was different for the clay fractions of W1 and W2. Both samples of W1 had a poorly resolved shoulder on the low-angle side of the peak near 9º2θ (10 Å), which is diagnostic of long-range ordering $R>1$ (Moore and Reynolds, 1997). Both samples of W2 had a well resolved shoulder at 11.7 Å, which shifted to 12.4 Å under EG solvation. All in all, the peaks were sharper and more intense in the case of W2 <0.6 µm, indicating a more ordered structure, unlike W1.

Table 5. Quantitative phase content of the bulk material and the 0.6−2 µm and <0.6 µm size fractions determined using Rietveld analysis.

Phase	Structure model *AutoQuan*®	Phase content (%)					
		W1 bulk	W2 bulk	W1 0.6−2 µm	W2 0.6−2 µm	W1 <0.6 µm	W2 <0.6 µm
Quartz	Quartz	43±2	46±2	12±1	7±1	2±1	2±1
Kaolinite	disordered kaolinite	21±3	20±2	42±5	51±5	55±5	60±5
Illite	Muscovite $2M_1$ Illite $1Mc$	20±2	19±2	24±2	22±3	21±3	19±3
Swellable components*	Smectite 1wCa#	12±3	11±3	17±3	16±3	18±3	16±4
Feldspar	Orthoclase	3±1	3±1	3±1	3±1	3±1	3±1
	Plagioclase An16						
Rutile	Rutile	1±1	1±1	2±1	1±1	1±1	0
Fe phases**		n.q.	n.q.	n.q.	n.q.	n.q.	n.q.

* discrete smectite + contribution from I-S mixed-layer minerals
** Goethite, hematite, marcasite, and siderite below XRD detection limits.
# Ca- rich dioctahedral smectite with one water layer, based on Ufer *et al.* (2004)
n.q.: not quantified.

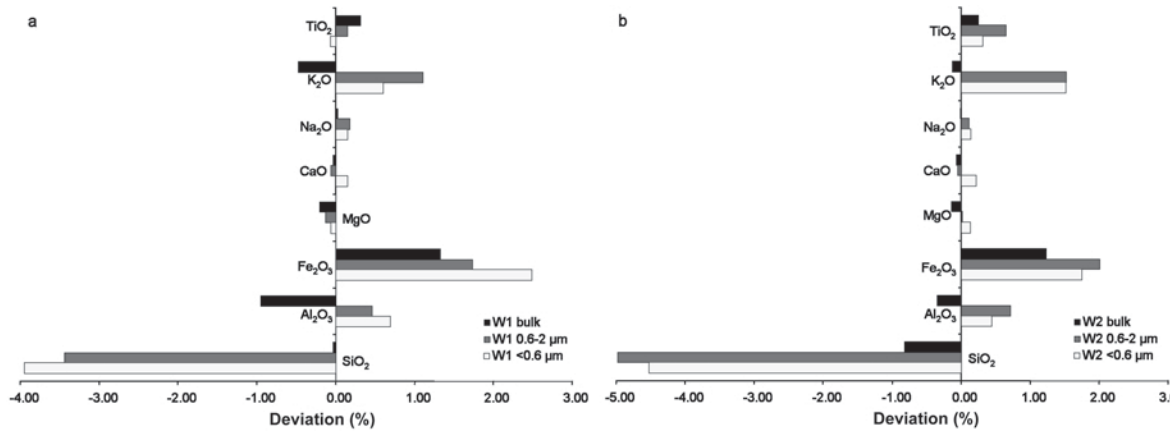

Figure 1. Relative deviation between chemical composition, calculated from Rietveld analysis and measured by XRF, for the bulk material and the clay fractions of samples (a) W1 and (b) W2.

Identification of the mixed-layer phases was carried out by ODPF. The experimental and the calculated XRD patterns (Figure 3) were compared using several structure models. A good coincidence of positions,

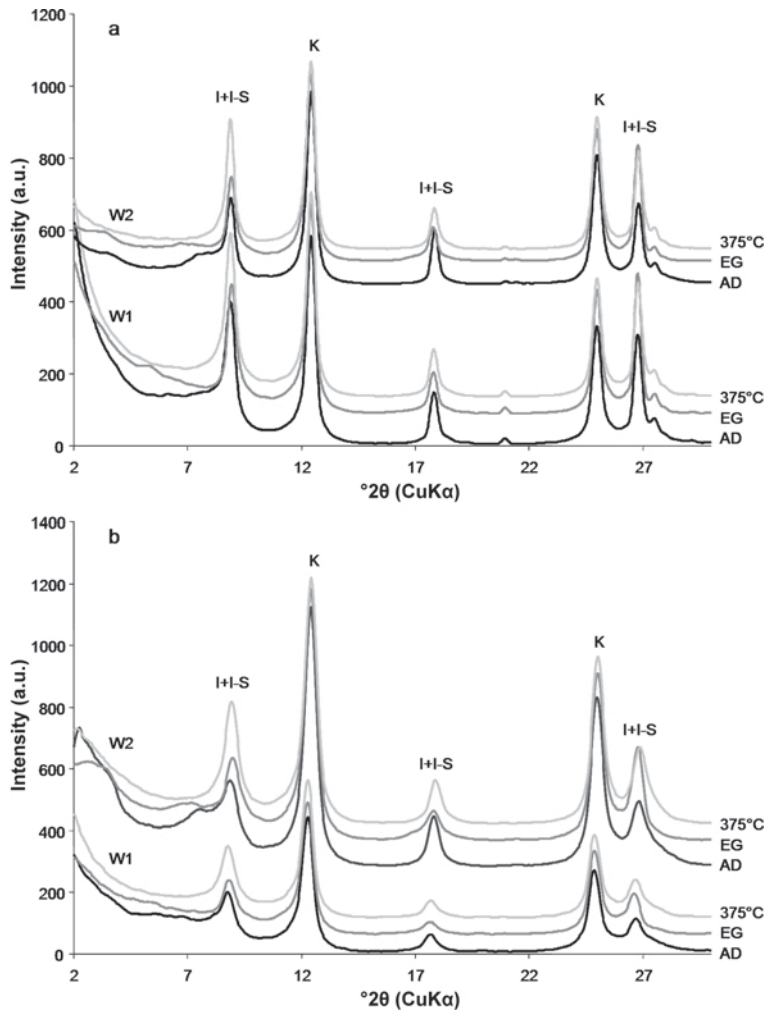

Figure 2. XRD patterns from oriented preparations. Comparison of samples W1 and W2 in the air-dried state (AD), after treatment with ethylene glycol (EG) and heating (375ºC) for the size fractions (a) 0.6−2 µm and (b) <0.6 µm.

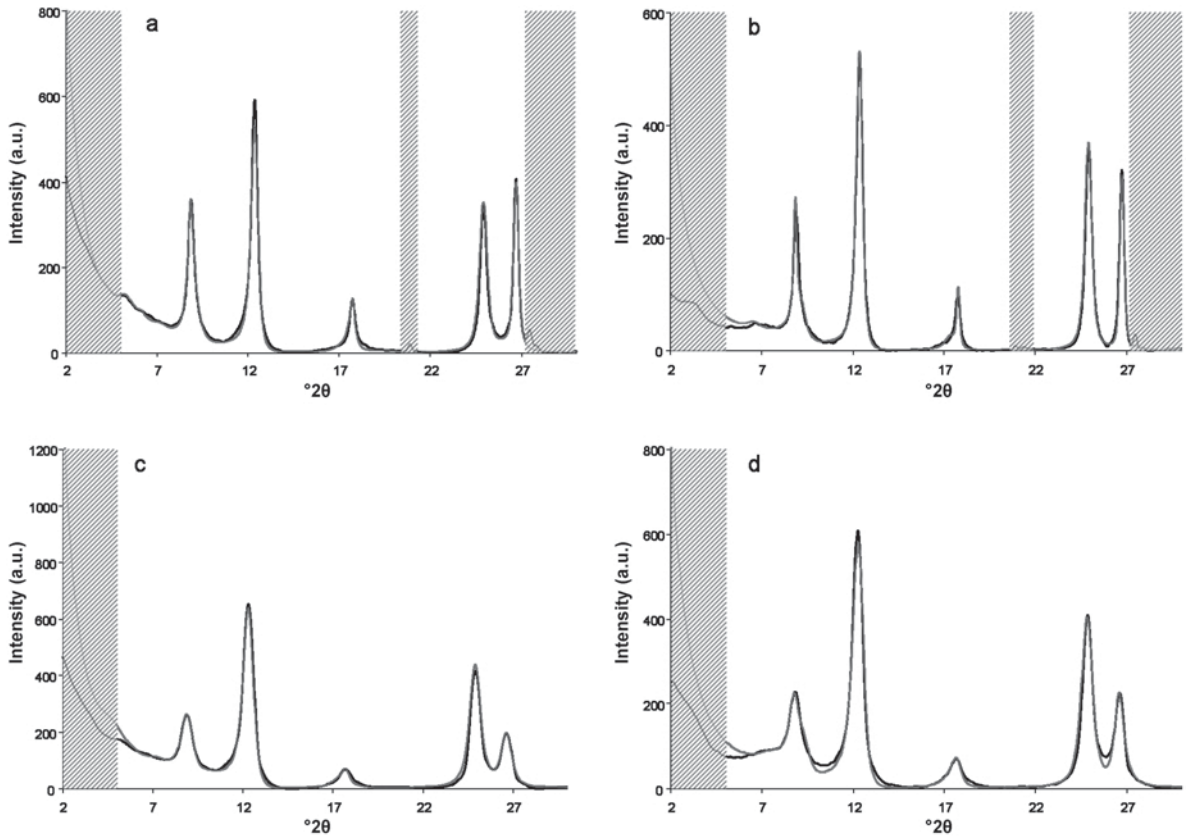

Figure 3. Experimental (black) and simulated (gray) XRD patterns of the Ca-saturated, EG-solvated samples from oriented preparations of the size fractions (a) W1, 0.6−2 μm, (b) W2, 0.6−2 μm, (c) W1, <0.6 μm, and (d) W2, <0.6 μm. The shaded areas were excluded from the fit.

intensities, and profiles was achieved for both clay samples with an I-S model, in which smectite and illite layers are interstratified with some tendency for segregation. Both experimental XRD patterns of the clay fractions of W1 were described successfully by a physical mixture of discrete smectite and R3 I(0.9)-S, whereas the clay fractions of W2 were characterized by a greater proportion of smectite in the mixed-layers (R1 I(0.85)-S for W2 0.6−2 μm and R1 I(0.80)-S for W2 <0.6 μm), but by smaller amounts of discrete smectite or no smectite in the case of W2 <0.6 μm (Table 6).

The accuracy of the fitting procedure was demonstrated by the satisfactory agreement between the experimental and calculated patterns, which was R_p = 7.14% for sample W1 0.6−2 μm and R_p = 7.20% for W2 0.6−2 μm, as well as R_p = 7.88% for W1 <0.6 μm and R_p = 8.71% for W2 <0.6 μm. Disagreement between experimental and calculated profiles was, however, observed for the low-angle part, probably because of the influence of instrumental factors and, in particular, Lorentz-polarization effects (Sakharov *et al*., 1999).

For both samples, the degree of structural disorder of kaolinite seemed high, as the diagnostic XRD peaks (data not shown) were so poorly resolved that no Hinckley index could be determined.

Simultaneous thermal analysis

From STA measurements, the maximum clay content was estimated by comparing the measured mass loss during dehydroxylation ($\Delta m\ T_{DHXmeas}$) between 400 and 900ºC from TG curves with a calculated mass loss ($\Delta m\ T_{DHXcalc}$) based on the quantification results from Rietveld analysis. The calculated mass loss is given by

$$\Delta m T_{DHXcalc} = x\frac{2M_{H_2O}}{M_{Kao}} + y\frac{M_{H_2O}}{M_{Smectite}} + z\frac{M_{H_2O}}{M_{Illite}} \quad (1)$$

Table 6. Quantification results from one-dimensional XRD profile fitting.

	W1 0.6−2 μm (%)	W2 0.6−2 μm (%)	W1 <0.6 μm (%)	W2 <0.6 μm (%)
Kaolinite	44	48	57	63
Smectite	4	2	4	0
I-S	31	19	32	22
−Reichweite	R3	R1	R3	R1
$-W_a$*	0.90	0.85	0.90	0.80
Illite	21	31	7	15

* W_a: portion of the component that appears at first in the mixed-layer mineral.

where x, y, and z are the coefficients of the respective mass fractions of kaolinite, the smectitic components, and illite gathered from Rietveld analysis. M is the molecular weight, assuming 18 g/mol for water, 258 g/mol for kaolinite, 375 g/mol for smectite, and 390 g/mol for illite. The estimation process was carried out for a range of coefficients (x, y, z), which comprised the mean values of each mass fraction, as well as their standard deviations (+s, −s). The success of estimation was proved by a delta value (Δ), subtracting $\Delta m\ T_{DHXcalc}$ from $\Delta m\ T_{DHX}$. An overestimation of the clay content by Rietveld analysis led to a negative Δ value. As $\Delta m\ T_{DHX}$ marks the upper limit, negative Δ values were discarded. Within the tested groups, the smallest positive Δ value indicated the most appropriate set of coefficients. The best match between calculated and experimental data was achieved for the bulk samples considering the mean values as coefficients (Table 7). For the clay fractions of W1 and W2, the smallest Δ values were obtained by a set of coefficients generated from negative standard deviations.

The mass loss during the dehydroxylation reaction ($\Delta m\ T_{DHX}$) was slightly greater for the bulk sample of W1. In case of the clay fractions, W2 showed somewhat larger values.

The DSC (differential scanning calorimetry) curves of both samples showed four endothermic and two exothermic transitions (Table 8). Except for the first dehydration reaction, the bulk material of W2 had slightly higher peak temperatures of thermal reaction than those of W1. For both clays, the peak of the second dehydration reaction was only resolved as a weak shoulder. Differences between the two samples were observed in the peak temperature of the recrystallization reaction, which was notably lower for W1 (958−974ºC) compared with W2 (975−981ºC). The recrystallization reaction of W1 varied with grain size, whereas it remained nearly constant for W2. In both sets of samples, the recrystallization peaks were neither sharp nor intense.

For the grain-size fraction <0.6 μm of W1 and W2, PA curves were recorded and compared with kaolinite-rich samples of different degrees of structural disorder (Figure 4). As thresholds, the data of a well ordered kaolinite (Mesa Alta) and of a highly disordered kaolinite (Franterre) were taken from Smykatz-Kloss (1974). The other samples employed were in-house standards used to discern device-specific effects. W1 and W2 plotted close to the PA curve of the disordered kaolinite sample, whereas W1 was closer than W2.

CEC measurements

Measured CEC values were 9 meq/100 g and 7 meq/100 g for the bulk samples of W1 and W2,

Table 7. Estimation of the maximum possible clay content by comparing the measured mass loss ($\Delta m\ T_{DHXmeas}$) during the dehydroxylation reaction with the calculated mass loss ($\Delta m\ T_{DHXcalc}$). x, y, and z are the average mass fractions with their standard deviations (−s, +s) of the 1:1 and 2:1 layer silicates from Rietveld analysis. Δ: deviation between measured and calculated mass loss $\Delta m\ T_{DHX}$.

Sample	Kaolinite x	Smectite + smectitic layers in mixed-layer minerals y	Illite + illitic layers in mixed-layer minerals z	$\Delta m\ T_{DHX\ calc}$ (%)	$\Delta m\ T_{DHX\ meas}$ (%)	Δ (%)
W1 bulk	0.21	0.12	0.20	4.43	4.52	0.09
W1 bulk −s	0.18	0.09	0.18	3.77	4.52	0.75
W1 bulk +s	0.24	0.15	0.22	5.08	4.52	−0.56
W2 bulk	0.20	0.11	0.19	4.19	4.31	0.12
W2 bulk −s	0.18	0.08	0.17	3.68	4.31	0.63
W2 bulk +s	0.22	0.14	0.21	4.71	4.31	−0.40
W1 0.6−2 μm	0.42	0.17	0.24	7.78	7.16	−0.62
W1 0.6−2 μm −s	0.37	0.14	0.22	6.85	7.16	0.31
W1 0.6−2 μm +s	0.47	0.20	0.26	8.72	7.16	−1.56
W2 0.6−2 μm	0.51	0.16	0.22	8.90	7.94	−0.96
W2 0.6−2 μm −s	0.46	0.13	0.19	7.92	7.94	0.02
W2 0.6−2 μm +s	0.56	0.19	0.25	9.88	7.94	−1.94
W1 <0.6 μm	0.55	0.18	0.21	9.50	8.98	−0.52
W1 <0.6 μm −s	0.50	0.15	0.18	8.52	8.98	0.46
W1 <0.6 μm +s	0.60	0.21	0.24	10.48	8.98	−1.50
W2 <0.6 μm	0.60	0.16	0.19	10.01	9.08	−0.93
W2 <0.6 μm −s	0.55	0.12	0.16	8.99	9.08	0.09
W2 <0.6 μm +s	0.65	0.20	0.22	11.04	9.08	−1.96

Table 8. Peak temperatures of thermal reactions from STA measurements of bulk materials and the clay fractions (0.6–2 μm and <0.6 μm).

Reaction Character Peak temperature	Dehydration, endothermic *T* (ºC)		Organic oxidation, exothermic *T* (ºC)	Dehydroxylation, endothermic *T* (ºC)	α→β-quartz transition, endothermic *T* (ºC)	Recrystallization, exothermic *T* (ºC)
W1	101	162	322	527	576	965
W2	92	163	347	532	576	981
W1 0.6–2 μm	104	169	328	544	n.o.	974
W2 0.6–2 μm	105	173	340	550	n.o.	980
W1 <0.6 μm	116	175	337	547	n.o.	958
W2 <0.6 μm	108	171	353	552	n.o.	975

n.o.: not observed

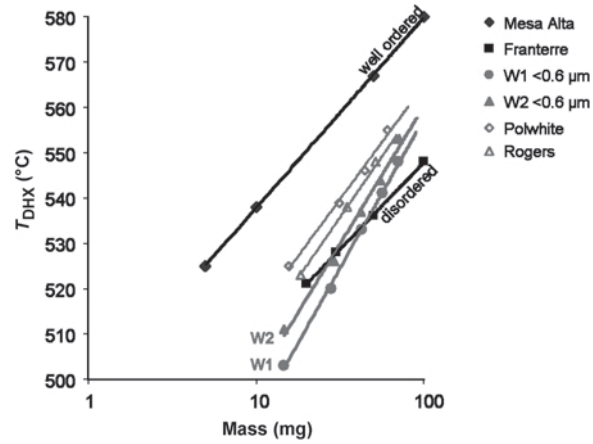

Figure 4. PA curves to estimate the degree of structural disorder of kaolinite of the samples W1<0.6 μm and W2<0.6 μm (bold gray lines). Bold black lines: PA curves of a well ordered and a disordered kaolinite as threshold references taken from Symkatz-Kloss (1974). Open markers: reference kaolinites.

respectively, and increased within the clay fractions (0.6–2 μm, <0.6 μm) from 10 meq/100 g to 19 meq/100 g for W1 and from 12 meq/100 g to 18 meq/100 g for W2.

The swellable components content (sum of smectite and smectitic layers in I-S) was calculated according to Lagaly (1993), assuming an average molecular weight M of 375 g/mol for smectites (Wolters, 2005), 10% variable charge, and a mean layer-charge density (χ) of 0.30 eq/formula unit (Kaufhold *et al*., 2002). In addition, kaolinite and illite were assumed to have a CEC of 5 meq/100 g (Kaufhold and Penner, 2006), giving rise to the expression

$$w_{sc} = \frac{CEC_{corr} M}{1000\chi} \quad (2)$$

where w_{sc} is the swellable components content (%) and CEC_{corr} is the cation exchange capacity after subtraction of 10% of variable charge and the kaolinite and illite contents determined from Rietveld analysis (Table 9).

Comparing the amount of exchanged cations in the exchanging solution with the CEC (Table 9) revealed that the interlayer of the swellable components is dominated by Ca^{2+} and Mg^{2+}. The sum of exchangeable cations (Σ) was in the range of the measured CEC for both sets of samples.

Microscopic techniques and Mössbauer spectroscopy

Investigation of the coarsest fraction (>63 μm) by optical microscopy revealed yellowish-brown, Fe-coated agglomerates to be abundant in W2 but rarely found in W1. Analysis by ESEM coupled with EDX confirmed that these coatings were rich in Fe. Sample W1 showed sporadic coatings consisting of crystals with a flat, tabular habit with "cockscomb" growth, typical of marcasite (Rösler, 1991).

Table 9. Amount of exchangeable cations and CEC measurements (CEC_{meas}) of the bulk material and the clay fractions 0.6−2 μm and <0.6 μm.

Cation	W1 bulk (meq/100 g)	W2 bulk (meq/100 g)	W1 0.6−2 μm (meq/100 g)	W2 0.6−2 μm (meq/100 g)	W1 <0.6 μm (meq/100 g)	W2 <0.6 μm (meq/100 g)
Na^+	0	0	0	0	0	0
Mg^{2+}	3	2	2	3	5	4
K^+	0	0	1	0	1	1
Ca^{2+}	7	5	6	6	12	12
Σ	10	7	9	9	18	17
CEC_{meas}	9	7	10	12	19	18
%CEC	111	100	90	76	95	97
CEC_{corr}	6	4	6	7	13	12
w_{sc} (%)	8	5	7	9	17	15

%CEC: ratio of the sum of exchangeable cations (Σ) to measured CEC.
CEC_{corr}: corrected CEC according to equation 2.
w_{sc}: swellable components content from CEC measurements.

The distribution of Fe was established by means of Mössbauer spectroscopy (Table 10). The bulk sample of W2 contained four times more oxide-bound Fe than did bulk sample W1. For sample W1, the ratio of silicate-bound Fe to oxide-bound Fe remained almost constant with decreasing grain size, whereas this ratio increased in the case of sample W2.

Summary of the quantification results

The layer silicate content of the ceramic clays W1 and W2 was determined by a multi-method approach, in order to crosscheck the quantification results from Rietveld analysis and ODPF (Table 11). To ensure comparability, only the portion of clay minerals from Rietveld analysis was considered. Therefore, ODPF results were normalized to the mean values (conv., norm. mv) from Rietveld analysis, as well as to the Rietveld quantification results after subtracting the standard deviation (conv., norm. −s). The four phases determined by ODPF (kaolinite, smectite, I-S, and illite) were converted to five phases (kaolinite, smectite, smectite layers, illite, and illite layers), subdividing the I-S content according to the respective W_a values. With the normalized ODPF values, the maximum mass loss $\Delta m\ T_{DHXcalc}$ was calculated according to equation 1 and compared with the measured results ($\Delta m\ T_{DHXmeas}$). For this calculation, the quantification results of the original four phases from ODPF were reduced to the three discrete 'end-member phases': kaolinite, smectite, and illite, adding together the smectite and smectite layers, and the illite and illite layers contents.

Table 10. Fe distribution, from Mössbauer spectroscopy, of the bulk materials and the <0.6 μm fractions.

	Silicate bound (%)	Oxide bound (%)
W1 bulk	88	12
W1 <0.6 μm	90	10
W2 bulk	49	51
W2 <0.6 μm	77	23

For sample W1 0.6−2 μm, the kaolinite content varied between 32 and 42% in the tested methods. For the appropriate Δ values, the smallest quantification result of 32% from ODPF equated to a large positive Δ value of 0.80 (always in combination with the other coefficients), denoting underestimation. A kaolinite content of 42% from Rietveld analysis (mean value) yielded the largest negative Δ value of −0.62, implying overestimation. Comparing the quantification results of all the clay-fraction samples, some general tendencies became evident: the strongest variability in phase content was noted for smectite, with Rietveld quantification results remarkably higher than those obtained by ODPF. The quantification results from Rietveld analysis (mv) always led to the largest negative Δ values; the largest positive Δ values were produced from results from ODPF (conv., norm. −s).

On the basis of the Δ value as an assessment tool for quantification, data sets generated from Rietveld analysis (−s) and ODPF (conv., norm. mv) were in the same range. Rietveld quantification results (mv) as well as the results from ODPF (conv., norm. −s) induced large Δ values, which indicated a greater inconsistency in the quantification results obtained from different methods.

The swellable components content from CEC measurements (Table 9) was closer to the results from ODPF in the case of both samples 0.6−2 μm, whereas for both samples <0.6 μm results were closer to those from Rietveld analysis.

DISCUSSION

Physical-chemical parameters

The influence of grain-size distribution as well as pH, electrical conductivity, and soluble-salt concentration on

Table 11. Quantification by Rietveld analysis and one-dimensional XRD profile modeling (ODPF) compared with the maximum mass loss Δm T_{DHX}.

Sample	Quantification method	Kaolinite (%)	Smectite (%)	Smectite layers (%)	Illite (%)	Illite layers	Σ (%)	Δm $T_{DHXcalc}$ (%)	Δm $T_{DHXmeas}$ (%)	Δ (%)
W1 0.6–2 μm	Rietveld mv	42	17	n.d.	24	n.d.	83	7.78	7.16	−0.62
	Rietveld −s	37	14	n.d.	22	n.d.	73	6.85	7.16	0.31
	ODPF	44	4	3	21	28	100	–	–	–
	ODPF conv., norm. mv	37	3	3	17	23	83	7.29	7.16	−0.13
	ODPF conv., norm. −s	32	3	2	15	21	73	6.36	7.16	0.80
W2 0.6–2 μm	Rietveld mv	51	16	n.d.	22	n.d.	89	8.90	7.94	−0.96
	Rietveld −s	46	13	n.d.	19	n.d.	78	7.92	7.94	0.02
	ODPF	48	2	3	31	16	100	–	–	–
	ODPF conv., norm. mv	43	2	3	27	14	89	8.13	7.94	−0.19
	ODPF conv., norm. −s	38	2	2	24	12	78	7.06	7.94	0.88
W1 <0.6 μm	Rietveld mv	55	18	n.d.	21	n.d.	94	9.50	8.98	−0.52
	Rietveld −s	50	15	n.d.	18	n.d.	83	8.52	8.98	0.46
	ODPF	57	4	3	7	29	100	–	–	–
	ODPF conv., norm. mv	53	4	3	7	27	94	9.42	8.98	−0.44
	ODPF conv., norm. −s	47	3	3	6	24	83	8.31	8.98	0.67
W2 <0.6 μm	Rietveld mv	60	16	n.d.	19	n.d.	95	10.01	9.08	−0.93
	Rietveld −s	55	12	n.d.	16	n.d.	83	8.99	9.08	0.09
	ODPF	63	0	4	15	18	100	–	–	–
	ODPF conv., norm. mv	59	0	4	14	17	95	9.93	9.08	−0.85
	ODPF conv., norm. −s	52	0	3	13	15	83	8.77	9.08	0.31

mv: mean value; −s: quantification value after subtracting the standard deviation; norm: normalized value; conv: converted value from phase reduction.
n.d.: not determinable with the respective method.

the processing properties of ceramic clay masses are discussed below.

Grain-size distribution (Table 3) depends heavily on the kind of dispersant and the method employed. The use of Na-pyrophosphate leads to a mass shift toward smaller particles sizes, which is caused by the destruction of aggregates and the formation of discrete particles. The adsorption of pyrophosphate on particles increases the negative charge and their dispersibility in water (Jeanroy and Guillet, 1981). The samples investigated responded very differently after Na-pyrophosphate treatment, and this cannot be explained by an electrostatic stabilization effect alone. Comparing the values of the different methods, the mass fraction of the sample W2 <0.6 μm without dispersant increased by a factor of ~10 after the treatment with Na-pyrophosphate. Simultaneously, the 0.6–2 μm fraction content was depleted to about a third. For sample W1, the redistribution of grain sizes with Na-pyrophosphate was less dramatic: the respective <2 μm fractions differed from each other by a factor of two. Microscopic investigations and Mössbauer spectroscopy (Table 10) showed differences in Fe distribution for the two samples. In the case of sample W1, the Fe was largely silicate bound, whereas for W2 it was mostly oxide bound. The greater oxide-bound Fe content in W2 is mainly reflected by the existence of yellowish-brown goethite-rich coatings, which tend to aggregate smaller particles together giving the impression of a larger grain size. The influence of Fe oxides on the aggregation behavior of clays is well known (*e.g.* Colombo and Torrent, 1991; Cornell and Schwertmann, 2003). Bascomb (1968) reported that pyrophosphate is able to extract Fe from moderately crystallized goethite. The application of pyrophosphate leads to the destruction of micro-aggregates and the dispersion of clayey and colloidal cements (Pansu and Gautheyrou, 2006). A summary of the mechanisms of the action of

pyrophosphate was given by Beckett (1989). According to Ongley *et al*. (1981), the different kinds of treatments give rise to an absolute grain-size distribution and to an effective grain-size distribution. The contrast between these two states plays an important role, as they both exert a strong influence on the rheological properties of clays, not only in ceramics but also in the paper industry (Grafton, 1968), and in sediment dynamics (Walling and Moorehead, 1989). Furthermore, the measuring method itself affects the results. The present data confirm that the Sedigraph method for particle-size analysis consistently estimates a finer size distribution than the pipette method (Buchan *et al*., 1993; Hotchkiss, 1994). However, independent of the measuring method, both data sets from treatment with and without Na-pyrophosphate illustrate the different aggregation characteristics of W1 and W2, which are jointly responsible for the processing properties.

Significant differences between the two samples are noticeable in the soluble-salt concentration. W1 releases >12 times as much sulfate, which is also reflected by the greater electrical conductivity. The sulfate release is probably caused by oxidation of marcasite (Rimstidt and Vaughan, 2003), as marcasite is the only sulfide-bearing mineral found in the samples. The greater SO_4^{2-} concentration in W1 is in accord with the observation of marcasite during the ESEM analysis. The small amount of sulfate released by W2, combined with the information from Mössbauer spectroscopy, plus the observation of yellowish-brown Fe-coatings, indicate that the Fe is largely oxide bound, presumably as goethite.

The larger soluble-salt concentration of W1 explains the greater degree of dispersibility of the raw material in water. Penner and Lagaly (2001) showed that multivalent anions up to high salt concentrations exert a pronounced liquefying effect on kaolinite-rich dispersions, as anions recharge the edges and cancel the edge(+)/face(−) interaction which result in a reduced viscosity (Rand and Melton, 1977).

The influence of pH on the clay suspensions cannot be taken into consideration for the different processing properties of W1 and W2, as the values are the same for both clays within standard deviation.

Kromer and Rose (1994) stated that increased amounts of swelling clay minerals prevent liquefaction of the clays, so that the differences in processing properties of W1 and W2, with respect to the extrusion pressure and 'making moisture' content, were made more complex by the interaction of the physical-chemical parameters with the mineralogical phase content.

Mineralogical parameters

Regarding the bulk samples, the deviations between the element oxides from XRF measurements and the oxide-converted Rietveld values were <0.5% for all tested element oxides. Larger deviations were noted for the SiO_2/Al_2O_3 ratio and in the Fe_2O_3 content for the two samples. The deviation in Fe_2O_3 content is explained by the fact that Fe-bearing phases at such low concentrations could not have been identified by XRD with CuKα radiation due to significant background fluorescence resulting in a poor peak resolution (Bland *et al*., 2004). Moreover, Mössbauer spectroscopy showed that some of the Fe is silicate bound, which again reduces the XRD-detectable portion.

Furthermore, indirect proof for the presence of silicate-bound Fe was provided by the generation of PA curves (Figure 4). Kaolinites with high degrees of structural disorder were found to contain more octahedral Fe(III) than those with well ordered structure (Herbillon *et al*., 1976; Mestdagh *et al*., 1980). The presence of very disordered kaolinite is also reflected in STA measurements by the weak recrystallization reaction at low temperatures. Such thermal behavior is typical of clays from Westerwald which are known to contain very disordered kaolinite (Lippmann, 1960; Jasmund and Lagaly, 1993). All of the methods tested indicated consistently that the kaolinite in sample W1 has a greater degree of structural disorder.

Deviations in the SiO_2/Al_2O_3 ratio were caused by the lack of an appropriate structural model for I-S mixed-layer minerals within the Rietveld method and correlation of clay mineral phases. This effect was emphasized for the clay fractions, where the SiO_2 content was overestimated and the Al_2O_3 content was underestimated consistently.

The clay-fraction samples of W1 and W2 showed positive deviations in terms of the K_2O content, implying underestimation of the K-bearing phases by Rietveld analysis. This may have been caused by an inappropriate illite structural model as well as by an incorrect quantification result for illite and/or orthoclase. The Rietveld quantification was carried out using a combination of two structural models (muscovite $2M_1$ and illite $1Mc$), because of the better fit. The oxide conversion was carried out on the basis of a high-K-illite structural model (0.89 K^+/formula unit (f.u.)) according to Środoń *et al*. (2002). Even when setting the stoichiometry to the maximum value of 1 K^+/f.u., the positive K_2O deviation decreases only slightly, suggesting an underestimation of illite and/or orthoclase by Rietveld analysis. An increase in the illite content together with a decrease in the feldspar content should be expected with decreasing particle size (Dultz, 2002). The results from the present Rietveld analysis showed nearly constant values for illite and feldspar within the various fractions, whereas ODPF showed an increase in the illite-layer content with decreasing particle size.

Balancing the deviations, a plausible explanation for the positive deviations in the Al_2O_3 and K_2O contents and the negative deviations of SiO_2 for the clay fractions is given by an overestimation of the smectitic components coupled with a simultaneous underestimation of

the kaolinite and illite content and/or feldspar content by Rietveld analysis. For the bulk material of W1 and W2, the quartz and kaolinite contents seem to be slightly underestimated, whereas the illite content and the amount of swellable components appear to be overestimated. The results from CEC measurements of both bulk samples and the 0.6−2 μm clay fractions reflect also the tendency to overestimate swellable components by Rietveld analysis. For both <0.6 μm clay fractions, the amounts of swellable components determined by CEC measurements and Rietveld analysis are very similar, while the results for the 0.6−2 μm samples match better with the contents gathered from ODPF. The results from STA measurements correspond, in the case of sample W1 <0.6 μm, slightly better with the results from ODPF, whereas for sample W2 <0.6 μm the results from STA measurements and Rietveld analysis correlate better.

However, both the structure and the amount of swellable minerals in ceramic clays influence significantly the water binding, the size of the delaminated particles and their spatial movement, and the distribution of the material during processing. Because of their smaller layer charge, in contrast to illite, the swellable components are thought to act like 'predetermined breaking-points'. The delamination behavior and the resulting water-accessible surfaces of R1 and R3 mixed-layer I-S minerals are compared to pure smectite in Figure 5. Delamination is expected to occur not only in suspensions, but also in wet ceramic clay masses under high shear stress, as applied during extrusion. According to this model, the plasticity of W1 is caused by the presence of discrete smectite which acts like a lubricant compensating the lower delamination potential of the R3 I-S particles. In contrast, the R1 I-S particles of W2 form stockier stacks of 2:1 layers by delamination, and these cannot enter interparticle spaces, resulting in lower plasticity during processing at the same operational load.

The greater plasticity of W1 results in a greater dry-bending strength and in an increased 'making moisture' content and extrusion pressure, which in turn, increase energy consumption during the drying and firing process.

CONCLUSIONS

The processing properties of ceramic clays are influenced by the interaction of different material parameters. The present study showed that the two ceramic clays investigated differed in terms of the following parameters: effective grain-size distribution, soluble-salt concentration, particle agglomeration by Fe coatings, the occurrence of discrete smectite, and the amount and degree of ordering of mixed-layer I-S minerals.

The qualitative delamination model deduced from the structural information gives an indication of how the swellable components may influence the processing properties of ceramic clays. With increasing amounts of swellable layers, the number of 'predetermined breaking points' increases, and so too, therefore, does the number of water-accessible surfaces. As a consequence, microstructural modifications are facilitated for clay systems containing larger amounts of swellable components, which may in turn result in greater plasticity.

Further studies are required to quantify the contribution of each parameter to workability, with special attention paid to the swellable components, as challenges remain in terms of the quantitative determination of all material parameters due to the small concentrations of components and/or inappropriate structural models for Rietveld quantification of mixed-layer minerals in complex mineral admixtures.

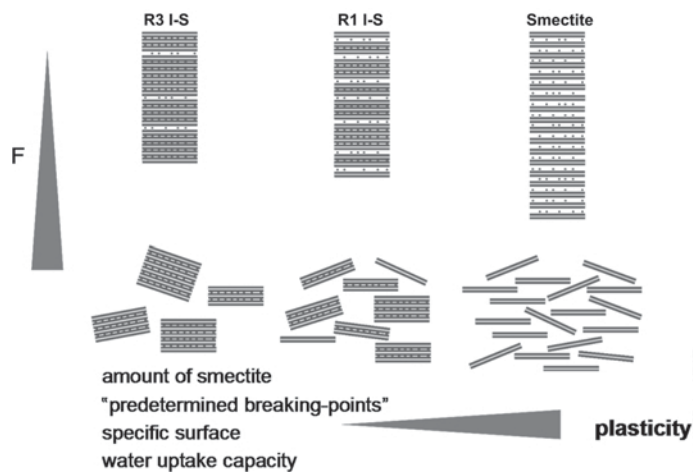

Figure 5. Relationship between the structure and ordering principle of 2:1 layer silicates and delamination behavior affecting processing properties.

Characterization of ceramic clays for the prediction of processing properties can be gained only by means of a multi-method approach as detailed information on the phase content seems to be the only way to elucidate the differences in ceramic clays that are graded as being the same according to traditional quality assessment of industrial raw clays.

ACKNOWLEDGMENTS

The authors are grateful to U. Wagner and F. Wagner (Technical University of Munich) for the Mössbauer spectroscopy; to N. Groschopf (University of Mainz) for the XRF measurements; to T. Cesny (WBB Fuchs) for sample preparation; to A. Steudel, H. Kaden, A. Buer, and E. Stefanescu (KIT) for sample preparation and general help in the laboratory; to F. Friedrich (KIT) for the ESEM investigations; to M. Heinle (KIT) for ICP-OES measurements; to E. Zeelmaekers and D. McCarty (Chevron Energy Technology Company, Houston, Texas, USA) for providing the *SYBILLA* program; and to S. Kaufhold (BGR, Hannover), K. Ufer, and R. Kleeberg (Technical University of Freiberg) for helpful discussions.

The study was financed by the German Ministry of Education and Research (BMBF), grant 01FR0626B.

REFERENCES

Bascomb, C.L. (1968) Distribution of pyrophosphate – extractable iron and organic carbon in soils of various groups. *Journal of Soil Science*, **19**, 251–268.

Beckett, P.H.T. (1989) The use of extractants in studies on trace metals in soils, sewage sludges, and sludge-treated soils., 143–176 in: *Advances in Soil Science* **9** (B.A. Stewart, editor). Springer-Verlag, Berlin.

Bergmann, J., Friedel, P., and Kleeberg, R. (1998) BGMN – A new fundamental parameters based Rietveld program for laboratory X-ray sources, its use in quantitative analysis and structure investigations. Commission of Powder Diffraction. *International Union of Crystallography CPD Newsletter* **20**, 5–8.

Bland, P.A., Cressey, G., and Menzies, O.N. (2004) Modal mineralogy of carbonaceous chondrites by X-ray diffraction and Mössbauer spectroscopy. *Meteoritics & Planetary Science* **39**, 3–16.

Buchan, G.D., Grewal, K.S., Claydon, J.J., and McPherson, R.J. (1993) A comparison of sedigraph and pipette methods for soil particle-size analysis. *Australian Journal of Soil Research*, **31**, 407–417.

Colombo, C. and Torrent, J. (1991) Relationship between aggregation and iron oxides in Terra Rossa soils from southern Italy. *Catena*, **18**, 51–59.

Cornell, R.M. and Schwertmann, U. (2003) *The Iron Oxides: Structure, Properties, Reactions, Occurrences, and Uses*. Wiley-VCH, Weinheim, Germany, 664 pp.

Crosby, N.T. and Patel, I. (1995) *General Principles of Good Sampling Practice*. The Royal Society of Chemistry, Cambridge, UK, pp. 68 .

DIN 19683-2 (1973) Physikalische Laboruntersuchungen – Bestimmung der Korngrößenzusammensetzung nach Vorbehandlung mit Natriumpyrophosphat.

DIN 38414-4 (1984) German standard methods for the examination of water, waste water and sludge; sludge and sediments (group S); determination of leachability by water (S 4)

Drits, V.A. (1987) Mixed-layer minerals: Diffraction methods and structural features. Pp. 33–45 in: *Proceedings of the International Clay Conference, Denver, 1985* (L.G. Schultz, H. van Olphen, and F.A. Mumpton, editors). The Clay Minerals Society, Bloomington, Indiana, USA.

Drits, V. and Sakharov, B.A. (1976) X-ray structural analysis of mixed-layer minerals. *Transactions of Academy of Sciences U.S.S.R.*, **295**, 252 *(in Russian)*.

Drits, V.A., Sakharov, B.A., Lindgreen, H., and Salyn, A.L. (1997) Sequential structure transformation of illite-smectite-vermiculite during diagenesis of Upper Jurassic shales from the Northern Sea and Denmark. *Clay Minerals*, **32**, 351–371.

Dultz, S. (2002) Effects of parent material and weathering on feldspar content in different particle size fractions from forest soils in NW Germany. *Geoderma*, **106**, 63–81.

Göhlert, K. and Uebel, M. (2007) Test method for plasticity and extrusion behaviour. Pp. 347–362 in: *Extrusion in Ceramics* (F. Händle, editor). Springer, Berlin.

Grafton, D.R. (1968) *The Effect of Clay-Adhesive Interaction on the Structure of Coatings*. The Institute of Paper Chemistry, Lawrence University, Wisconsin, USA, 104 pp.

Herbillon, A.J., Mestagh, M.M., Vielvoye, L., and Derouane, E.G. (1976) Iron in kaolinite with special reference to kaolinite from tropical soils. *Clay Minerals*, **11**, 201–220.

Hinckley, D.N. (1963) Variability in crystallinity values among the kaolin deposits of the coastal plain of Georgia and South Carolina. *Clays and Clay Minerals*, **11**, 229–235.

Hofmann, U. (1962) Die Tonminerale und die Plastizität des Tons. *Keramische Zeitschrift*, **14**, 14–19.

Hotchkiss, R. (1994) *Evaluation of pipet and X-ray procedures for determining particle-size distributions of sediment*. U.S. Geological Survey, Office of Water Data Coordination, 28 pp.

Howard, S.A. and Preston, K.D. (1989) Profile fitting of powder diffraction patterns. Pp. 217–276 in: *Modern Powder Diffraction* (D.L. Bish and J.E. Post, editors). Reviews in Mineralogy, **20**, Mineralogical Society of America, Washington, D.C.

Jasmund, K. and Lagaly, G. (1993) *Tonminerale und Tone: Struktur, Eigenschaften, Anwendungen und Einsatz in Industrie und Umwelt*. Steinkopff, Darmstadt, Germany, 490 pp.

Jeanroy, E. and Guillet, B. (1981) The occurrence of suspended ferruginous particles in pyrophosphate extracts of some soil horizons. *Geoderma*, **26**, 95–105.

Kaufhold, S. and Penner, D. (2006) Applicability of the SER method for quality control of clays from the German 'Westerwald'. *Applied Clay Science*, **32**, 53–63.

Kaufhold, S., Dohrmann, R., Ufer, K., and Meyer, F.M. (2002) Comparison of methods for the quantification of montmorillonite in bentonites. *Applied Clay Science*, **22**, 145–151.

Kleeberg, R. (2009) State-of-the-art and trends in quantitative phase analysis of geological and raw materials. *Zeitschrift für Kristallographie, Supplement*, **30**, 47–52.

Koster van Groos, A.F. and Guggenheim, S. (1984) The effect of pressure on the dehydration reaction of interlayer water in Na-montmorillonite (SWy-1). *American Mineralogist*, **69**, 872–879.

Krolla-Sidenstein, P., Kaden, R., Emmerich, K., Petrick, K., He, L., and Gliemann, H. (2009) Methods characterising microbial community composition during clay maturation. *14th International Clay Conference*, Vol. 2 (S. Fiore, C. Belviso, and M.L. Giannossi, editors), Bari, Italy, p. 20.

Kromer, H. (1979) Rohstoffmerkblätter der Deutschen Keramischen Gesellschaft e.V. *Berichte der Deutschen Keramischene Gesselschaft* (1968–1979).

Kromer, H. (1980) Tertiary clays in the Westerwald area. *Geologisches Jahrbuch, Reihe D* **Heft D39**, 69–84.

Kromer, H. and Rose, D. (1994) Der Einfluß des

Stoffbestandes auf das Verflüssigungsverhalten von Tonen. *Berichte der Deutschen Keramischen Gesellschaft*, **71**, 245–249.

Kromer, H. and Schüller, K.-H. (1973) Eigenschaften von Kaolinen für die Keramik und als Füllstoff. *Berichte der Deutschen Keramischen Gesellschaft*, **50**, 39–41.

Lagaly, G. (1993) Layer charge determination by alkylammonium ions. Pp. 2–46 in: *Layer Charge Characteristics of 2:1 Silicate Clay Minerals* (A.R. Mermut, editor). CMS Workshop Lectures, **6**, The Clay Minerals Society, Bloomington, Indiana, USA.

Lanson, B., Sakharov, B.A., Claret, F., and Drits, V. (2009) Diagenetic smectite-to-illite transition in clay-rich sediments: A reappraisal of X-ray diffraction results using the multi-specimen method. *American Journal of Science*, **6**, 476–516.

Lindgreen, H., Drits, V., Sakharov, B.A., Salyn, A.L., Wrang, P., and Dainyak, L.G. (2000) Illite-smectite structural changes during metamorphism in Cambrian Alum shales from the Baltic sea. *American Mineralogist*, **85**, 1223–1238.

Lippmann, F. (1960) Über eine Apparatur zur Differentialthermoanalyse (DTA). *Keramische Zeitschrift*, **11**, 475–480, 524–528, 570–573.

Liu, C.-L., Hart, N., and Peck, Jr. H.D. (1982) Inorganic pyrophosphate: Energy source for sulfate-reducing bacteria of the Genus *Desulfotomaculum*. *Science*, **23**, 363–364.

Loomis, G.A. (1938) Grain size of whiteware clays as determined by the Andreasen pipette. *Fortieth Annual Meeting of the American Ceramic Society*, 393–399.

McCarty, D.K., Drits, V.A., Sakharov, B.A., Zviagina, B.B., Ruffell, A., and Wach, G. (2004) Heterogeneous mixed-layer clays from the Cretaceous greensand, Isle of Wight, southern England. *Clays and Clay Minerals*, **52**, 552–575.

McCarty, D.K., Sakharov, B.A., and Drits, V.A. (2008) Early clay diagenesis in gulf coast sediments: New insights from XRD profile modeling. *Clays and Clay Minerals* **56**, 359–379.

Meier, L.P. and Kahr, G. (1999) Determination of the cation exchange capacity (CEC) of clay minerals using the complexes of copper (II) ion with triethylenetetramine and tetraethylenepentamine. *Clays and Clay Minerals*, **47**, 386–388.

Menger-Krug, E., Kaden, R., Krolla-Sidenstein, P., Emmerich, K., Petrick, K., and Obst, U. (2008) Biological processes during maturation. In *4th Mid-European Clay Conference* (A. Skowroński, editor), Kraków, Poland, p. 113.

Mestagh, M.M., Vielvoye, L., and Herbillon, A.J. (1980) Iron in kaolinite: II. The relationship between kaolinite crystallinity and iron content. *Clay Minerals*, **15**, 1–13.

Moore, D.M. and Reynolds, R.C. Jr. (1997) *X-ray Diffraction and the Identification and Analysis of Clay Minerals*. Oxford University Press, New York, 378 pp.

Murray, H.H. (2000) Traditional and new applications for kaolin, smectite, and palygorskite: A general overview. *Applied Clay Science*, **17**, 207–221.

Omotoso, O., McCarty, D.K., Hillier, S., and Kleeberg, R. (2006) Some successful approaches to quantitative mineral analysis as revealed by the 3rd Reynolds Cup Contest. *Clays and Clay Minerals* **54**, 748–760.

Ongley, E.D., Bynoe, M.C., and Percival, J.B. (1981) Physical and geochemical characteristics of suspended solids, Wilton Creek, Ontario. *Canadian Journal of Earth Science*, **18**, 1365–1379.

Pansu, M. and Gautheyrou, J. (2006) *Handbook of Soil Analysis*. Springer-Verlag, Berlin, 993 pp.

Penner, D. and Lagaly, G. (2001) Influence of anions on the rheological properties of clay mineral dispersions. *Applied Clay Science*, **19**, 131–142.

Petrick, K., Emmerich, K., Menger-Krug, E., Kaden, R., Dieterle, M., Kuch, P., Diedel, R., Peuker, M., and Krolla-Sidenstein, P. (2008) Why do two apparently similar German ceramic clays display different rheological properties during maturation? *4th Mid-European Clay Conference*, (A. Skowroński, editor), Kraków, Poland, p. 128.

Rand, B. and Melton, I.E. (1977) Particle interactions in aqueous kaolinite suspensions: I. Effect of pH and electrolyte upon the mode of particle interaction in homoionic sodium kaolinite suspensions. *Journal of Colloid and Interface Science*, **60**, 308–320.

Rieder, M., Cavazzini, G., D'Yakonov, Y.S., Frank-Kamenetskii, V.A., Gottardi, G., Guggenheim, S., Koval, P.V., Müller, G., Neiva, A.M.R., Radoslovich, E.W., Robert, J.-L., Sassi, F.P., Takeda, H., Weiss, Z., and Wones, D.R. (1998) Nomenclature of the micas. *Clays and Clay Minerals*, **46**, 586–595.

Rimstidt, J.D. and Vaughan, D.J. (2003) Pyrite oxidation: A state-of-the-art assessment of the reaction mechanism. *Geochimica et Cosmochimica Acta*, **67**, 873–880.

Rösler, H.J. (1991) *Lehrbuch der Mineralogie*. Deutscher Verlag für Grundstoffindustrie, Leipzig, Germany, 844 pp.

Sakharov, B.A., Lindgreen, H., Salyn, A.L., and Drits, V.A. (1999) Determination of illite-smectite structures using multispecimen X-ray diffraction profile fitting. *Clays and Clay Minerals*, **47**, 555–566.

Schejbal, F. (1978) Westerwälder Tone heute, Teil 4: Der Wettbewerb, die Zukunftsaussichten. *Keramische Zeitschrift*, **30**, 362–364.

Schmidt, H. (1981) Neuere Erkenntnisse über den Einfluss des Mineralbestandes auf die stofflichen Eigenschaften von grobkermischen Massen und Erzeugnissen. *Fortschrift für Mineralogie*, **59**, 227–266.

Schüller, K.-H. (1980) Die Bedeutung untergeordneter Bestandteile bei technologischen Prozessen. *Fortschrift für Mineralogie*, **58**, 79–105.

Smykatz-Kloss, W. (1974) *Differential Thermal Analysis*. Springer-Verlag, Berlin, 185 pp.

Środoń, J. (1981) X-ray identification of randomly interstratified illite-smectite in mixtures with discrete illite. *Clay Minerals*, **16**, 297–304.

Störr, M. (1983) Die Kaolinlagerstätten der Deutschen Demokratischen Republik. In: *Schriftenreihe für geologische Wissenschaften*, Vol. 18. Akademie Verlag.

Störr, M. and Schwerdtner, G. (1979) Geologie, Mineralogie und Technologie der DDR. *Zeitschrift für Angewandte Geologie*, **25**, 505–514.

Ufer, K., Roth, G., Kleeberg, R., Stanjek, H., Dohrmann, R., and Bergmann, J. (2004) Description of X-ray powder pattern of turbostratically disordered layer structures with a Rietveld compatible approach. *Zeitschrift für Kristallographie*, **219**, 519–527.

Ufer, K., Kleeberg, R., Bergmann, J., and Dohrmann, R. (2009) Structurally based modelling of the X-ray diffraction patterns of illite/smectite mixed-layer minerals within the Rietveld method. *14th International Clay Conference*, Vol. **1** (S. Fiore, C. Belviso, and M. L. Giannossi, editors), Bari, Italy, p. 408.

Vogt, S. and Vogt, R. (2004) Relationship between minerals and the industrial manufacturing properties of natural clay deposits and the clay bodies produced from them for the heavy clay industry: Part 2. Manufacturing properties, utilization estimates and clay body optimization. Pp. 78–103 in: *Z.I.-Ziegelindustrie International Jahrbuch* (W. Müller and A. Fischer, editors).

Wagner, F.E. and Kyek, A. (2004) Mössbauer spectroscopy in archeology: Introduction and experimental considerations. *Hyperfine Interactions*, **154**, 5–33.

Walling, D.E. and Moorehead, P.W. (1989) The particle size characteristics of fluvial suspended sediment: An overview.

Hydrobiologia, **176**/**177**, 125–149.
Whitney, G. and Northrop, H.R. (1987) Diagenesis and fluid flow in the San Juan Basin, New Mexico – regional zonation in the mineralogy and stable isotope composition of clay minerals in sandstone. *American Journal of Science*, **287**, 353–382.
Wiegmann, J., Kranz, G., Horte, C.-H., Graul, J., and Doberenz, C. (1978) Beziehungen zwischen den petrologischen Charakteristika und den keramisch-technischen Eigenschaften von Kaolinen mit nennenswerten Gehalten an Illit-Smectit-Wechsellagerungsmineralen. *Silikattechnik*, **29**, 263–267.
Winkler, H.G.F. (1954) Bedeutung der Korngrößenverteilung auf die stofflichen Eigenschaften grobkeramischer Erzeugnisse. *Berichte der Deutschen Keramischene Gesselschaft*, **31**, 337–343.
Wolters, F. (2005) Classification of montmorillonites. PhD thesis, Universität Karlsruhe, Germany, pp. 169.
Wolters, F., Lagaly, G., Kahr, G., Nüesch, R., and Emmerich, K. (2009) A comprehensive characterization of dioctahedral smectites. *Clays and Clay Minerals*, **57**, 115–133.
Zeelmaekers, E., McCarty, D.K., and Mystkowski, K. (2007) *SYBILLA*. Chevron Energy Technology Company, Houston, Texas.

(*Received 29 July 2010; revised 15 February 2011; Ms. 465; A.E. W.D. Huff*)